European Journal of Medicinal Chemistry 214 (2021) 113241

Contents lists available at ScienceDirect

European Journal of Medicinal Chemistry

journal homepage: http://www.elsevier.com/locate/ejmech

# Synthesis and preliminary anticancer evaluation of new triazole bisphosphonate-based isoprenoid biosynthesis inhibitors

Thibaut Legigan [a, **], Evelyne Migianu-Griffoni [a], Mohamed Abdenour Redouane [a], Aurélie Descamps [a], Julia Deschamp [a], Olivier Gager [a], Maëlle Monteil [a], Florent Barbault [b], Marc Lecouvey [a, *]

[a] Université Sorbonne Paris Nord, UMR-CNRS 7244, Laboratoire Chimie, Structures, Propriétés de Biomatériaux et d'Agents Thérapeutiques (CSPBAT), équipe Chimie Bioorganique et Synthèse, 1 rue de Chablis, 93000, Bobigny, France
[b] Université de Paris, ITODYS, CNRS, F-75006, Paris, France

ARTICLE INFO

*Article history:*
Received 21 December 2020
Received in revised form
25 January 2021
Accepted 25 January 2021
Available online 2 February 2021

*Keywords:*
Cancer
Chemotherapy
1-Hydroxymethylene-1,1-bisphosphonic acid
Click chemistry
Mevalonate pathway inhibition

ABSTRACT

The synthesis of a new set of triazole bisphosphonates **8a-d** and **9a-d** presenting an alkyl or phenyl substituent at the C-4 or C-5 position of the triazole ring is described. These compounds have been evaluated for their antiproliferative activity against MIA PaCa-2 (pancreas), MDA-MB-231 (breast) and A549 (lung) human tumor cell lines. 4-hexyl- and 4-octyltriazole bisphosphonates **8b-c** both displayed remarkable antiproliferative activities with $IC_{50}$ values in the micromolar range (0.75–2.4 μM) and were approximately 4 to 12-fold more potent than zoledronate. Moreover, compound **8b** inhibits geranylgeranyl pyrophosphate biosynthesis in MIA PaCa-2 cells which ultimately led to tumor cells death.


## 1. Introduction

Nitrogen-containing bisphosphonates (N-BPs) such as zoledronate **1**, risedronate **2** or alendronate **3** (Scheme 1a) are extensively indicated for the treatment of osteoporosis, Paget's disease of bone, hypercalcemia and bone metastases derived from breast and prostate primary tumors [1]. In addition to their essential role in the management of skeletal disorders, N-BPs also exhibit promising anticancer properties such as inhibition of tumor cell proliferation [2–5], induction of apoptosis, γδ T cell activation and inhibition of tumor cell invasion and migration both in vitro and in vivo [6]. The inherent antitumor activity of zoledronate **1**, one of the most potent N-BPs to date, has been also evaluated in phase III clinical trials. In these studies, administration of zoledronate **1** in combination with standard chemotherapy improves disease-free survival in post-menopausal women with early breast cancers [7] and increases the overall survival of patients with multiple myeloma [8].

N-BPs exert their antitumor properties by inhibiting farnesyl pyrophosphate synthase (FPPS) [9], a key enzyme of the mevalonate pathway involved in the synthesis of $C_{15}$ farnesyl pyrophosphate (FPP) from $C_5$ isoprenoids dimethylallyl pyrophosphate (DMAPP) and isopentenyl pyrophosphate (IPP - Scheme 1b). FPPS inhibition by N-BPs further impairs the biosynthesis of longer isoprenoids such as $C_{20}$ geranylgeranyl pyrophosphate (GGPP) which is produced by condensation between FPP and IPP catalyzed by geranylgeranyl pyrophosphate synthase (GGPPS) [10]. Both FPP and GGPP are implicated in protein prenylation, a post-translational modification required for the membrane anchoring and function of small GTPases (Ras, Rho, Rap or Rac) which play an essential role in cell signaling and proliferation and cell survival. FPPS inhibitors usually display a 1-hydroxymethylene-1,1-bisphosphonic acid (HMBP) scaffold which bind to the magnesium cations present in the active site of the enzyme. Moreover, a positively charged nitrogen atom in their side chains is also involved in hydrogen bonds with the hydroxyl group of Thr201 and the carbonyl moiety of Lys 200 in the allylic site of FPPS [11]. These interactions allow N-BP to mimic the carbocationic intermediate

* Corresponding author.
** Corresponding author.
*E-mail addresses:* thibaut.legigan@univ-paris13.fr (T. Legigan), marc.lecouvey@univ-paris13.fr (M. Lecouvey).

https://doi.org/10.1016/j.ejmech.2021.113241
0223-5234/

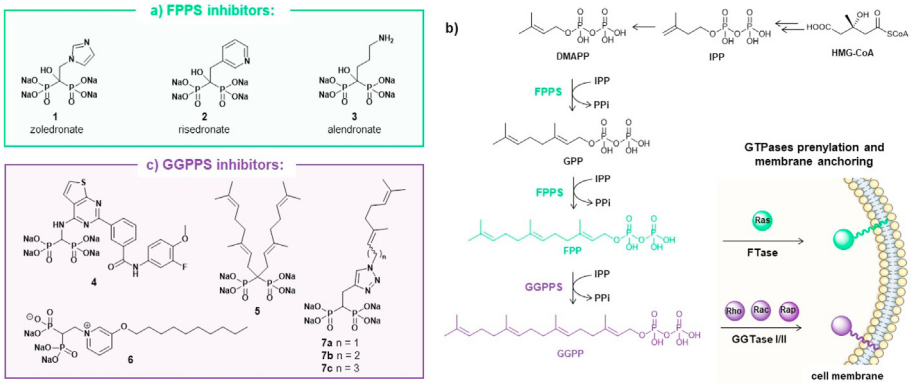


**Scheme 1.** – **a)** Structures of FPPS inhibitors zoledronate **1**, risedronate **2** and alendronate **3 in their fully deprotonated form**. **b)** Biosynthesis of the isoprenoids FPP and GGPP involved in the protein prenylation. **c)** Structures of the selective GGPPS inhibitors **4**, **5**, **6** and **7a-c**.

formed during the condensation of isoprenoid substrates catalyzed by FPPS [12].

Recently, disruption of GTPases geranylgeranylation induced by direct GGPPS inhibition also emerged as a promising approach for the treatment of cancer. Despite the lack of information on the structure of human GGPPS, a growing number of potent and selective GGPPS inhibitors has been described in the literature (Scheme 1c) [13]. Most of these compounds present a methylene-1,1-bisphosphonic acid moiety substituted by an extended heteroaromatic scaffold (compound **4** [14]) or lipophilic side chains (compounds **5** [15] and **6** [16]) which bind to large hydrophobic sub-pockets of the enzyme. According to this strategy, Wiemer et al. have developed the potent and selective GGPPS inhibitor **7b**, for which an isoprenoid chain was incorporated to a bisphosphonate moiety *via* a triazole linkage. Although the homoneryl isomer of **7b** (Z isomer – $IC_{50\ GGPPS} = 0.075\ \mu M$; $IC_{50\ FPPS} = 33.3\ \mu M$) was approximately 2-fold more potent than the homogeranyl isomer (E isomer – $IC_{50\ GGPPS} = 0.173\ \mu M$; $IC_{50\ FPPS} = 49.6\ \mu M$) [17], a mixture of homogeranyl and homoneryl isomers in a 3/1 ratio was identified as the most potent and selective GGPPS inhibitor to date ($IC_{50\ GGPPS} = 0.045\ \mu M$; $IC_{50\ FPPS} = 28\ \mu M$) [18]. Besides, **7b** (E/Z ~ 3/1) exhibits a potent antiproliferative effect on the multiple myeloma cell line RPMI-8226 ($EC_{50} = 0.19\ \mu M$) and significantly slows pancreatic tumor growth in mice [19]. This remarkable activity was attributed to a simultaneous binding of each Z and E isomers to the FPP substrate and GGPP product pockets of the enzyme [17]. It was also noted that both isomers of **7a** (n = 1) [20] and **7c** (n = 3) [21] were much less active than **7b** against human GGPPS, suggesting that inhibitory activity of triazole bisphosphonates **7** is strongly influenced by the structure of its lipophilic side chain.

Over the last years, our team has shown a keen interest in the anticancer properties of bisphosphonates [22]. In this article, we describe the synthesis and the preliminary biological evaluation of a new library of potential isoprenoid biosynthesis inhibitors **8a-d** and **9a-d** (Fig. 1). These compounds combine: 1) a 1-hydroxymethylene-1,1-bisphosphonic acid (HMBP) moiety which has proved to be essential for the biological activity of clinically approved FPPS inhibitors such as zoledronate **1** and 2) a triazole heterocyclic scaffold substituted respectively at the C-4 (**8a-d**, in blue) or C-5 position (**9a-d**, in orange) by hydrophobic alkyl chains or phenyl ring [23]. Although access of heterocyclic bisphosphonates such as **4** or **7a-c** often requires elaborated synthetic strategies [14,24] bisphosphonates **8a-d** and **9a-d** were conveniently synthesized through metal catalyzed 1,3-dipolar cycloaddition "click" reactions between commercially available or easily producible alkynes and azides. Moreover, the use of the triazole heterocycle in medicinal chemistry has attracted a considerable attention in recent years [25]. Thanks to their structural characteristics, such as polarity, rigidity, and their ability to act as both hydrogen bond donors and acceptors, triazoles are also considered as hydrolytically stable bioisosteres of amides, esters, alkene or imidazole [26]. Thus, this "click" chemistry approach would allow us to determine the influence of the substitution pattern of the triazole ring on the biological activity of compounds **8a-d** and **9a-d**.

## 2. Results and discussion

### 2.1. Chemistry

The synthesis of compounds **8a-d** is depicted in Scheme 2. First, 1,4-disubstituted triazoles **12a-d** were prepared through a copper(I)-catalyzed azide alkyne cycloaddition (CuAAC) [27] between methyl 2-azidoacetate **10** and the corresponding alkynes **11**. These CuAAC reactions were performed in the presence of $CuSO_4$ (10 mol%) and sodium ascorbate (10 mol%) in a mixture of THF and water, affording triazoles **12a-d** in 81–97% yields. Methyl esters **12a-d** were then subjected to saponification with aqueous NaOH in methanol at reflux to afford **13a-d** in 87–99% yields. With carboxylic acids **13a-d** in hand, we next turned our attention to the construction of the HMBP moiety of compounds **8a-d**. Although different methods are described in the literature, preparation of the HMBP scaffold generally relies on the condensation of a carboxylic acid with $H_3PO_3$ and $PCl_3$ or $POCl_3$. [28] This method often requires harsh acidic conditions, elevated temperatures, extended reaction times and cannot be carried out in the presence of sensitive functional groups. Therefore, compounds **8a-d** were prepared under mild conditions according to the methodology previously

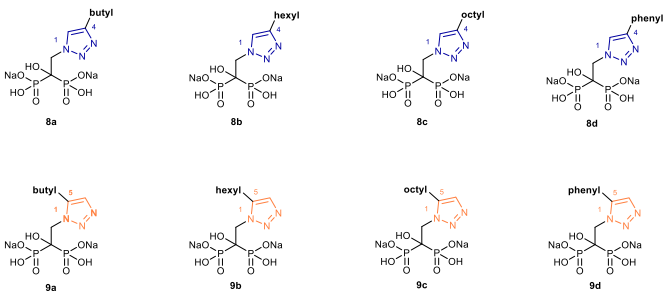


**Fig. 1.** - Structures of 1,4- and 1,5-disubstituted triazole bisphosphonates **8a-d** and **9a-d** described in this study.

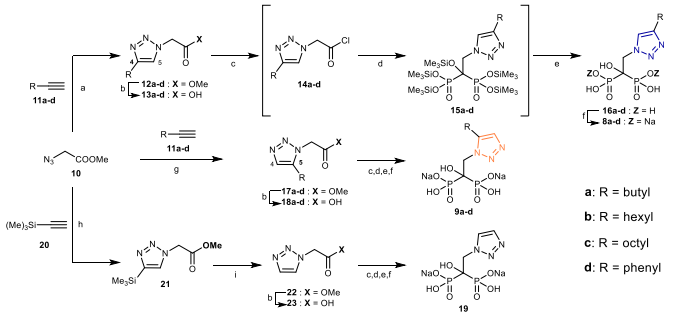


**Scheme 2.** – Synthesis of HMBP **8a-d**, **9a-d** and **18**. Reagents and conditions: a) $CuSO_4 \cdot 5H_2O$ (10% mol.), sodium ascorbate (10% mol.), THF/$H_2O$ 1/1, RT, 18 h, 81–97%; b) aqueous 1 M NaOH (6 equiv.), MeOH, reflux, 30 min, **13a-d**: 87–99% yield, **18a-d**: 79–100% yield, **23**: 87% yield; c) $(COCl)_2$, DCM, 0 °C, 15 min. d) $P(OSiMe_3)_3$ (3 equiv.), THF, 0 °C to RT, 50 min; e) MeOH, RT, 16 h; f) aqueous 0.2 M NaOH (2 equiv.), $H_2O$, RT, **8a-d**: 40–47% yield after 4 steps, **9a-d**: 24–55% yield after 4 steps, **19**: 48% yield after 4 steps. g) $Cp^*RuCl(PPh_3)_3$ (5% mol.), dioxane, 65 °C, 18 h, 66–89%; h) $CuSO_4 \cdot 5H_2O$ (4% mol.), sodium ascorbate (16% mol.), *t*-BuOH/$H_2O$ 1/2, RT, 12 h, 82%; i) AcOH (1.4 equiv.), TBAF (1 M in THF, 1.4 equiv.), THF, 0 °C to RT, 36 h, 84%.

developed by our group [29]. First, **13a-d** were converted to their corresponding acyl chlorides **14a-d** in the presence of oxalyl chloride in dichloromethane. Then, addition of $P(OSiMe_3)_3$ onto **14a-d** in dry THF at 0 °C smoothly furnished the silylated bisphosphonates **15a-d**. In this case, the complete consumption of the acyl chlorides **14a-d** was achieved in less than 1 h by using a slight excess amount (3 equivalents) of $P(OSiMe_3)_3$. After evaporation of the volatile fractions, a subsequent methanolysis step of the phosphonosilaesters **15a-d** led to 1-hydroxymethylene-1,1-bisphosphonic acids **16a-d** which were easily purified by precipitation in a mixture of methanol and acetone. 1-hydroxymethylene-1,1-bisphosphonic acids **16a-d** were then neutralized with an aqueous solution of NaOH led to HMBPs **8a-d** as disodium salts in 40–47% yield with a purity of ~98%.

A similar synthetic approach was used for the preparation of 1,5-triazole HMBPs **9a-d**. Cycloaddition between azide **10** and alkynes **11a-d** catalyzed by $Cp^*RuCl(PPh_3)_3$ in dioxane at 65 °C afforded **17a-d** in good to excellent yields (66–89%) [30]. The exclusive formation of 1,5-substituted triazole regioisomers was confirmed by $^{13}C$ NMR and HSQC experiments (see the ESI) [31]. A characteristic chemical shift of $C_4$ ($\delta$ ~ 132 ppm) was observed for 1,5-disubstituted triazoles **17a-d**, while the shift of $C_5$ for 1,4-triazoles **12a-d** was about 122 ppm. Saponification of methyl esters **17a-d** furnished **18a-d** which were directly converted to their corresponding HMBPs **9a-d** at similar yields (24–55%) following the previously described methodology.

We also prepared the monosubstituted triazole HMBP **19** [32] to investigate the importance of substituents at C-4 or C-5 position of the triazole ring for the biological activity of HMBPs **8a-d** and **9a-d**. Surprisingly, reaction between methyl 2-azidoacetate **10** and trimethylsilylacetylene **20** under the previously described CuAAC conditions afforded triazole **21** in only 7% yield, along with the formation of desilylated triazole **22** (8% yield). Nevertheless, cycloaddition between **10** and **20** in the presence of $CuSO_4$,$5H_2O$ (4% mol.) and sodium ascorbate (16% mol.) in a mixture of *tert*-butanol and water as described by Somsák et al. [33] cleanly provided triazole **21** as a sole product in a yield of 82%. Desilylation of **21** in the presence of TBAF and acetic acid in THF followed by saponification of the methyl ester **22** furnished the carboxylic acid **23**. Finally, the monosubstituted triazole HMBP **19** was obtained in 48% yield from **23**.

**Table 1**
$IC_{50}$ (μM)[a] of HMBPs **8a-d, 9a-d** and **18** determined by MTT cell viability assays.

| Compound | MIA PaCa-2 | MDA-MB-231 | A549 |
|---|---|---|---|
| **1** | 9.1 | 10.1 | 8.8 |
| **8a** | 28.9 | 32.7 | 22.9 |
| **8b** | 0.75 | 2.4 | 1.7 |
| **8c** | 1.0 | 1.2 | >100 |
| **8d** | >100 | >100 | 97.9 |
| **9a** | 95.3 | >100 | >100 |
| **9b** | 13.0 | 12.8 | 23.7 |
| **9c** | >100 | >100 | >100 |
| **9d** | >100 | >100 | >100 |
| **19** | >100 | >100 | >100 |

[a] These values represent the means of n ≥ 3 experiments performed in triplicate with standard deviation of ≤ 2-fold.

## 2.2. Antiproliferative activity on tumor cell lines

Antiproliferative effects of HMBPs **8a-d** and **9a-d** have been evaluated against MIA PaCa-2 (pancreas), MDA-MB-231 (breast) and A549 (lung) human tumor cell lines. Zoledronate **1**, a potent FPPS inhibitor with promising antiproliferative activity on a wide range of human cancer cell lines, was used as control. Cancer cells were treated with tested compounds at various concentrations for 72 h and cell viability was measured by MTT assay. As shown in Table 1, 4-butyltriazole **8a** exhibited weak antiproliferative effect against the three cancer cell lines ($IC_{50}$ = 22.9–32.7 μM), however, elongation of the triazole alkyl side chain dramatically affects cancer cell viability. For instance, 4-hexyltriazole **8b** displayed remarkable antiproliferative activities with $IC_{50}$ values in the micromolar range (0.75–2.4 μM) and was approximately 4 to 12-fold more potent than zoledronate at inhibiting cancer cells growth ($IC_{50}$ of 8.8–10.1 μM). 4-Octyltriazole **8c** exhibited similar antiproliferative activities than **8b** toward MIA PaCa-2 and MDA-MB-231 cells ($IC_{50}$ = 1.0 μM and 1.2 μM, respectively) but was essentially inactive against A549 cells. 4-Phenyltriazole **8d** and HMBP **19**, a zoledronate analog for which the imidazole ring was substituted by a triazole heterocycle, exerted no significant antiproliferative action on the three cancer cell lines, indicating that a long alkyl chain at the C-4 position of the triazole ring is required for the anticancer activity of **8b-c**. Transferring the C-4 alkyl chain of **8b-c** to the C-5 position of the triazole ring also led to a dramatic reduction in potency. Hence, HMBP **9b** was 5–17 less potent at inhibiting cancer cell growth than its regioisomer **8b** with $IC_{50}$ values of 13.0 μM, 12.8 μM and 23.7 μM against MIA PaCa-2, MDA-MB-231 and A549 tumor cells, respectively. Finally, HMBP **9a**, **9c** and **9d** showed no significant effects on cancer cell growth at the highest tested concentration of 100 μM.

We next decided to evaluate the antiproliferative effect of HMBP **24** (Fig. 2) to gain additional insights into structural features contributing to the growth-inhibitory potency of our lead triazole HMBP **8b** (synthesis of **24** is described in the ESI). **24** is a position isomer of **8b** for which the methylene group between the HMBP moiety and the triazole ring has been replaced by a propylene linker. Increasing the distance between the triazole ring and the HMBP scaffold also resulted in a dramatic reduction in potency (cell growth inhibition <30% at the highest tested concentration of 100 μM).

We then sought to confirm that the remarkable antiproliferative effect of HMBP **8b** on MIA PaCa-2 cancer cells ($IC_{50}$ = 0.75 μM) was the consequence of the isoprenoid biosynthesis inhibition. For this purpose, MIA PaCa-2 cells were incubated with **8b** in the presence or absence of FPP and GGPP precursors such as farnesol (FOH) and geranylgeraniol (GGOH) which were found to diffuse through the cell membrane and to restore GTPase prenylation *via* salvage pathway [34]. As illustrated in Fig. 3, HMBP **8b** induced a significant antiproliferative effect at the concentration of 2 μM on MIA PaCa-2

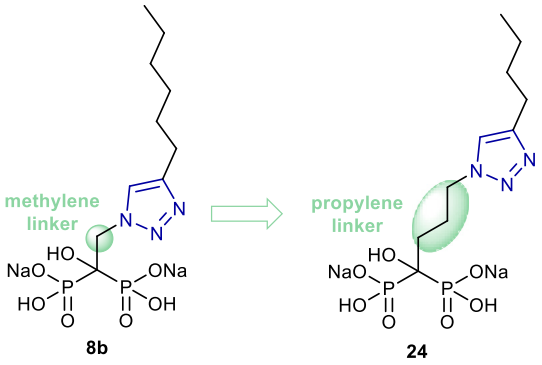


**Fig. 2.** – Structure of HMBP **24**.

cancer cells (70% cell growth inhibition). Co-incubation of **8b** (2 μM) with FOH at a non-toxic concentration (50 μM) did not restore the viability of cancer cells (60% growth inhibition). In stark contrast, the antiproliferative effect of **8b** is significantly reversed by addition of the mevalonate pathway metabolite GGOH (50 μM) in the culture medium (27% cell growth inhibition), confirming that HMBP **8b** inhibits the isoprenoid biosynthesis in MIA PaCa-2 cells which ultimately led to impairment of protein prenylation and cell death. Many studies shown that the toxicity of selective GGPPS inhibitors is reversed when cancer cells were co-treated with geranylgeraniol (GGOH) and not with farnesol (FOH). [14,16], However, a similar trend was also observed with the selective FPPS inhibitor zoledronate **1**, suggesting that antiproliferative effect of **1** could be at least partially attributed to inhibition of GTPases geranylgeranylation [35]. In our case, triazole HMBPs **8a-d** and **9a-d** are unlikely to act as a cationic transition-state analog inhibitor of human FPPS because the [1–3]-triazole heterocycle (pKa = 1.2) [36] is not basic enough to be protonated at physiological pH. It could be reasonably assumed that HMBP **8b**, which is structurally close to the triazole bisphosphonate **7** with its neutral, long and lipophilic side chain, directly impairs intracellular GGPP level through direct inhibition of GGPPS. To verify this hypothesis, we decided to perform a molecular docking study to explore potential binding mode of our triazole HMBP within the human GGPPS enzyme.

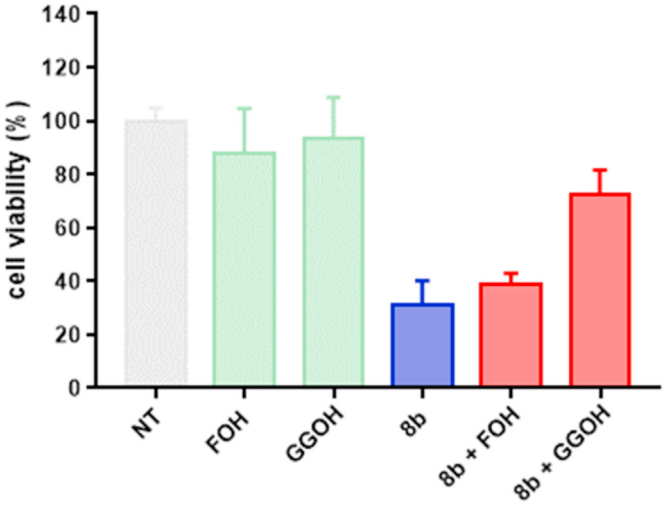


**Fig. 3.** – Effect of **8b** (2 μM) on MIA-PaCa-2 cell proliferation in the presence or absence of FOH (50 μM) or GGOH (50 μM).

### 2.3. Molecular docking

Prior to the docking computations, a structural investigation of the GGPPS protein structure was made through a molecular dynamics simulation and described in the ESI. Extensive molecular docking computations were then undertaken on the active site of GGPPS for the triazole HMBPs **8a-d** and **9a-d**. Molecular docking energies and clustering percentages are available on supplementary material (table S1). A notable result is the highly similar location of the bisphosphonate moieties for either **8a-d** or **9a-d** compounds. The negatively charged HMBP scaffold guides the association with GGPPS through favorable electrostatic interaction toward the magnesium ions and the positively charged residues Arg73, Lys 151 and Lys 212 (see Fig. 4). The 1,4-triazole ring gains two hydrogen bonds with the sidechain of Gln185 and Arg73. These favorable interactions guide the long alkyl chains at the C-4 position of the compounds **8b** and **8c** to fit into a large lipophilic pocket of human GGPPS as shown on Fig. 4. Superimposition of the docking poses with GGPP (in purple color on Fig. 4) bound to human GPPS (PDB: 2Q80) [10] confirmed that **8b** and **8c** could inhibit GGPPS by mimicking the C20 isoprenoid GGPP in the inhibitory binding pocket of the enzyme (Fig. 4). In stark contrast, alkyl substituents at C-5 position such as **9c** (Fig. 4) induce a translation of the triazole ring so that the hydrogen bond with Gln185 is removed and the alkyl chain is not fully incorporated in the GGPPS binding pocket. This bended geometry is possibly correlated with the reduced anticancer activities of these bisphosphonates. Previous computer modeling and crystallographic studies suggest that bisphosphonate inhibitors such as **7b** bind either to the GGPP site (inhibition site) or FPP site (substrate site) of GGPPS. [14,37], As a consequence, exact binding mode of triazole HMBPs **8b-c** needs to be confirmed by crystallographic investigation.

## 3. Conclusion

In this study, alkyl- and phenyl-substituted 1,4- and 1,5-triazole HMBPs **8a-d** and **9a-d** were conveniently synthesized with excellent regioselectivity and good yields using both copper and ruthenium azide-alkyne 1,3-dipolar cycloaddition. Preliminary biological evaluation of these compounds showed that HMBP **8b** inhibited isoprenoid biosynthesis in vitro and displayed promising antiproliferative effect against MIA PaCa-2, MDA-MB-231 and A549 cancer cell lines with $IC_{50}$ values in the micromolar range (0.75–2.4 μM). Furthermore, **8b** is approximately 4 to 12-fold more potent at inhibiting tumor cells growth than zoledronate **1**, an HMBP drug currently marketed for the treatment of bone

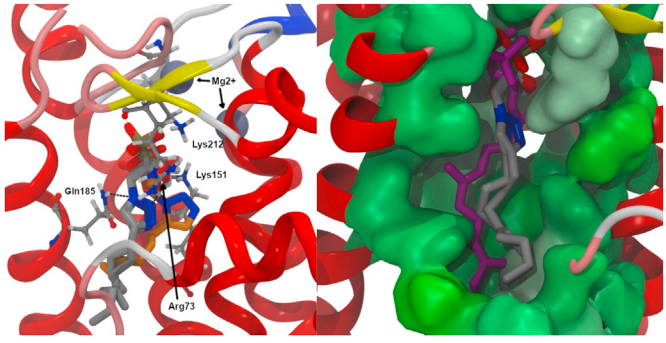


**Fig. 4.** - Left, molecular interactions of compounds **8b** and **8c** (carbon in grey) and compound **9c** (carbon in orange) with human GGPPS. Protein residues are displayed with balls and sticks and hydrogen bonds with dashed lines. Right, molecular surface of the binding pocket of GGPPS colored according to their hydrophobicity (green: hydrophobic to blue: hydrophilic). The GGPP compound, extracted from pdb code 2Q80 [10], is presented in purple.

metastases of breast and lung tumors. Structure-activity relationship study revealed that the antiproliferative activity of compound **8b** is highly dependent on both the presence of a long linear alkyl chain containing at least 6 carbon atoms at C-4 position of the triazole ring and the distance between the triazole heterocycle and the HMBP moiety. Molecular docking suggests that triazoles **8b** and **8c** bearing long alkyl chains could inhibit GGPP biosynthesis which led to disruption of GTPase geranyl-geranylation by filling the lipophilic inhibitory pocket of GGPPS. Overall, these results clearly showed that triazole HMBPs such as **8b** is an attractive lead for the development of new potent HMBP-based isoprenoid synthase inhibitors with improved anticancer properties.

## 4. Experimental section

### 4.1. General chemistry methods

All the reactions were performed in flame-dried glassware under argon atmosphere. All chemicals were purchased from Sigma-Aldrich and Alfa Aesar and were used as delivered. NMR spectra were recorded at room temperature on a Bruker Avance-III-400 spectrometer ($^{1}$H: 400 MHz, $^{13}$C: 101 MHz, $^{31}$P: 162 MHz). Chemical shifts ($\delta$) are reported in parts per million (ppm) and coupling constants (J) are reported in hertz (Hz). Standard abbreviations indicating multiplicity are used as follows: b = broad, s = singlet, d = doublet, t = triplet, m = multiplet. $^{31}$P NMR spectra were measured with $^{1}$H coupling. The reaction progress was monitored by $^{31}$P NMR experiments (spectra were recorded without lock and shims) or thin-layer chromatography on Macherey-Nagel Alugram Sil G/UV$_{254}$ precoated silica gel TLC plates. Spots were visualized by dipping the TLC plates into a solution of $KMnO_4$ in water following by heating with a heat gun. Flash column chromatography separations were performed using Macherey-Nagel silica gel 60 (15–40 μm) as the stationary phase. Mass spectra (MS) were recorded in negative (ESI$^-$) or positive mode (ESI$^+$) by using an Agilent 1260 Infinity II LC system coupled to an Agilent InfinityLab LC/MSD detector. High-resolution mass spectra (HRMS) were performed on a Bruker maXis mass spectrometer in negative (ESI$^-$) mode by the "Fédération de Recherche" ICOA/CBM (FR2708) platform (Université d'Orléans).

### 4.2. Synthesis of methyl 2-azidoacetate **10**

$NaN_3$ (9.87 g, 152 mmol, 1.1 eq.) was added to a solution of methyl chloroacetate (15 g, 138 mmol, 1.0 eq.) in DMF (138 mL). The mixture was stirred for 48 h and water (150 mL) was added. The aqueous layer was extracted with $Et_2O$ (3 × 150 mL). The organic layers were combined, washed with water (4 × 150 mL), dried over $MgSO_4$ and evaporated to afford methyl 2-azidoacetate **10** (12.55 g, 79% yield) as a colorless oil. $^{1}$H NMR (400 MHz, $CDCl_3$, 298 K): $\delta$ ppm = 3.87 (s, 2H), 3.78 (s, 3H). $^{13}$C NMR (100 MHz, $CDCl_3$, 298 K): $\delta$ ppm = 168.9, 52.7, 50.3. Spectral data are in agreement with those previously reported in the literature [38].

### 4.3. Synthesis of triazoles **12a-d**

$CuSO_4 \cdot 5H_2O$ (10 mol%) and sodium ascorbate (10 mol%) were successively added to a solution of azide **10** (1.2 eq.) and alkyne **11a-d** (1.0 eq.) in THF/$H_2O$ 1/1 ([alkyne] = 0.18 M). The mixture was stirred at room temperature for 18 h and THF was removed *in-vacuo*. The resulting aqueous layer was diluted with water (20 mL) and extracted with $CH_2Cl_2$ (3 × 20 mL). The combined organic layers were dried over $MgSO_4$ and evaporated. Triazoles **12a-d** were obtained after purification by chromatography over silica gel (petroleum ether/AcOEt 50/50).

Compound **12a**. Colorless oil (1.909 g, 97% yield). $R_f$: 0.56 (petroleum ether/AcOEt 50/50). $^{1}$H NMR (400 MHz, $CDCl_3$, 298 K): $\delta$ ppm = 7.39 (s, 1H), 5.11 (s, 2H), 3.76 (s, 3H), 2.70 (t, 2H, $^{3}J$ = 7.7 Hz), 1.67–1.60 (m, 2H), 1.40–1.31 (m, 2H), 0.90 (t, 3H, $^{3}J$ = 7.3 Hz). $^{13}$C NMR (100 MHz, $CDCl_3$, 298 K): $\delta$ ppm = 167.1, 148.9, 122.1, 53.0, 50.6, 31.5, 25.4, 22.3, 13.9. Spectral data are in agreement with those previously reported in the literature [39].

Compound **12b**. Colorless oil (1.832 g, 81% yield). $R_f$: 0.63 (petroleum ether/AcOEt 50/50). $^{1}$H NMR (400 MHz, $CDCl_3$, 298 K): $\delta$ ppm = 7.40 (s, 1H), 5.13 (s, 2H), 3.79 (s, 3H), 2.72 (t, 2H, $^{3}J$ = 7.7 Hz), 1.71–1.63 (m, 2H), 1.39–1.24 (m, 6H), 0.87 (t, 3H, $^{3}J$ = 7.0 Hz). $^{13}$C NMR (100 MHz, $CDCl_3$, 298 K): $\delta$ ppm = 167.1, 149.0, 122.1, 53.0, 50.7, 31.6, 29.3, 28.9, 25.7, 22.6, 14.1. MS (ESI): $[M+H]^+$ calcd for $C_{11}H_{20}N_3O_2^+$: 226.2; found: 226.1.

Compound **12c**. Colorless oil (2.453 g, 97% yield). $R_f$: 0.82 (petroleum ether/AcOEt 50/50). $^{1}$H NMR (400 MHz, $CDCl_3$, 298 K): $\delta$ ppm = 7.39 (s, 1H), 5.11 (s, 2H), 3.75 (s, 3H), 2.69 (t, 2H, $^{3}J$ = 7.7 Hz), 1.71–1.57 (m, 2H), 1.37–1.17 (m, 10H), 0.83 (t, 3H, $^{3}J$ = 6.9 Hz). $^{13}$C NMR (100 MHz, $CDCl_3$, 298 K): $\delta$ ppm = 167.0, 148.9, 122.1, 53.0, 50.6, 31.9, 29.4 (2C), 29.3, 29.2, 25.7, 22.7, 14.1. MS (ESI): $[M+H]^+$ calcd for $C_{13}H_{24}N_3O_2^+$: 254.2; found: 254.1.

Compound **12d**. White solid (1.030 g, 95% yield). $R_f$: 0.57 (petroleum ether/AcOEt 9/1). $^{1}$H NMR (400 MHz, $CDCl_3$, 298 K): $\delta$ ppm = 7.91 (s, 1H), 7.84 (d, 2H, $^{3}J$ = 7.8 Hz), 7.42 (t, 2H, $^{3}J$ = 7.8 Hz), 7.34 (t, 1H, $^{3}J$ = 7.8 Hz), 5.21 (s, 2H), 3.80 (s, 3H). $^{13}$C NMR (100 MHz, $CDCl_3$, 298 K): $\delta$ ppm = 166.8, 148.3, 130.4, 128.9 (2C), 128.4, 125.8 (2C), 121.2, 53.1, 50.8. Spectral data are in agreement with those previously reported in the literature.[36]

### 4.4. Synthesis of triazoles **17a-d**

A solution of azide **10** (1 eq.) and alkyne **11a-d** (1 eq.) in degassed 1,4-dioxane ([alkyne] = 0.9 M) was added to a solution of Cp*RuCl(PPh$_3$)$_3$ (5 mol%) in 1,4-dioxane ([Cp*RuCl(PPh$_3$)$_3$] = 0.009 M) under argon atmosphere. The mixture was stirred at 65 °C for 18 h and the solvent was removed *in-vacuo*. Triazoles **17a-d** were obtained after purification by chromatography over silica gel (petroleum ether/AcOEt 80/20).

Compound **17a**. Yellow oil (104 mg, 76% yield). $R_f$: 0.55 (petroleum ether/AcOEt (50/50). $^{1}$H NMR (400 MHz, $CDCl_3$, 298 K): $\delta$ ppm = 7.50 (s, 1H), 5.09 (s, 2H), 3.79 (s, 3H), 2.57 (t, 2H, $^{3}J$ = 7.7 Hz), 1.72–1.61 (m, 2H), 1.46–1.34 (m, 2H), 0.94 (t, 3H, $^{3}J$ = 7.3 Hz). $^{13}$C NMR (100 MHz, $CDCl_3$, 298 K): $\delta$ ppm = 166.8, 138.6, 132.1, 53.1, 48.8, 29.9, 22.9, 22.3, 13.8. MS (ESI): $[M+H]^+$ calcd for $C_9H_{16}N_3O_2^+$: 198.1; found: 198.1.

Compound **17b**. Yellow oil (103 mg, 66% yield). $R_f$: 0.45 (petroleum ether/AcOEt (50/50). $^{1}$H NMR (400 MHz, $CDCl_3$, 298 K): $\delta$ ppm = 7.49 (s, 1H), 5.08 (s, 2H), 3.79 (s, 3H), 2.56 (t, 2H, $^{3}J$ = 7.8 Hz), 1.69–1.61 (m, 2H), 1.42–1.23 (m, 6H), 0.88 (t, 3H, $^{3}J$ = 6.8 Hz). $^{13}$C NMR (100 MHz, $CDCl_3$, 298 K): $\delta$ ppm = 166.9, 138.5, 132.2, 53.1, 48.7, 31.5, 28.9, 27.8, 22.6, 23.2, 14.1. MS (ESI): $[M+H]^+$ calcd for $C_{11}H_{20}N_3O_2^+$: 226.2; found: 226.1.

Compound **17c**. Yellow oil (157 mg, 89% yield). $R_f$: 0.57 (petroleum ether/AcOEt (50/50). $^{1}$H NMR (400 MHz, $CDCl_3$, 298 K): $\delta$ ppm = 7.49 (s, 1H), 5.08 (s, 2H), 3.79 (s, 3H), 2.56 (t, 2H, $^{3}J$ = 7.8 Hz), 1.70–1.62 (m, 2H), 1.41–1.21 (m, 10H), 0.88 (t, 3H, $^{3}J$ = 6.7 Hz). $^{13}$C NMR (100 MHz, $CDCl_3$, 298 K): $\delta$ ppm = 166.9, 138.4, 132.4, 53.1, 48.7, 31.9, 29.3 (2C), 29.2, 27.9, 23.2, 22.8, 14.2. MS (ESI): $[M+H]^+$ calcd for $C_{13}H_{24}N_3O_2^+$: 254.2; found: 254.1.

Compound **17d**. Yellow oil (111 mg, 73% yield). $R_f$: 0.47 (petroleum ether/AcOEt 50/50). $^{1}$H NMR (400 MHz, $CDCl_3$, 298 K): $\delta$ ppm = 7.75 (s, 1H), 7.51–7.48 (m, 3H), 7.39–7.36 (m, 2H), 5.13 (s, 2H), 3.76 (s, 3H). $^{13}$C NMR (100 MHz, $CDCl_3$, 298 K): $\delta$ ppm = 167.2, 139.0, 133.1, 130.0, 129.3 (2C), 128.8 (2C), 126.6, 53.1, 49.2. MS (ESI): $[M+Na]^+$ calcd for $C_{11}H_{11}N_3O_2Na^+$: 240.1; found: 240.1.

### 4.5. Synthesis of TMS-substituted triazole **21**

$CuSO_4 \cdot 5H_2O$ (85 mg, 0.34 mmol, 4 mol%) and sodium ascorbate (269 mg, 1.36 mmol, 16 mol%) were successively added to a solution of TMS-acetylene **19** (999 mg, 10.17 mmol, 1.2 eq.) and azide **10** (976 mg, 8.48 mmol, 1.0 eq.) in *t*-BuOH/$H_2O$ 1/2 (60 mL). The mixture was stirred at room temperature for 12 h and was diluted with water (50 mL). The resulting aqueous layer was extracted with AcOEt (3 × 50 mL). The combined organic layers were dried over $MgSO_4$ and evaporated. Triazole **20** (1.480 g, 82% yield, white solid) was obtained after purification by chromatography over silica gel (EP/AcOEt 50/50). Rf: 0.61 (petroleum ether/AcOEt 50/50). $^1$H NMR (400 MHz, $CDCl_3$, 298 K): $\delta$ ppm = 7.66 (br s, 1H), 5.20 (s, 2H), 3.80 (s, 3H), 0.33 (s, 9H). $^{13}$C NMR (100 MHz, $CDCl_3$, 298 K): $\delta$ ppm = 167.1, 147.3, 130.4, 53.1, 50.2, −1.1 (3C). MS (ESI): $[M+H]^+$ calcd for $C_5H_{16}N_3O_2Si^+$: 214.1; found: 214.0.

### 4.6. Synthesis of monosubstituted triazole **22**

Acetic acid (230 μL, 4.00 mmol, 1.4 eq.) and TBAF (1 M in THF, 4 mL, 4.00 mmol, 1.4 eq.) were successively added to a cooled solution of TMS-substituted triazole **20** (610 mg, 2.86 mmol, 1.0 eq.) in dry THF (14.7 mL). The mixture was stirred at room temperature for 36 h and THF was removed *in-vacuo*. The crude was purified by chromatography over silica gel (petroleum ether/AcOEt 20/80) to afford triazole **21** (339 mg, 84% yield) as a white solid. $R_f$: 0.30 (petroleum ether/AcOEt 50/50). $^1$H NMR (400 MHz, $CDCl_3$, 298 K): $\delta$ ppm = 7.76 (s, 1H), 7.73 (s, 1H), 5.22 (s, 2H), 3.80 (s, 3H). $^{13}$C NMR (100 MHz, $CDCl_3$, 298 K): $\delta$ ppm = 167.0, 134.3, 125.1, 53.1, 50.6. MS (ESI): $[M+H]^+$ calcd for $C_5H_8N_3O_2^+$: 142.1; found: 142.0.

### 4.7. Synthesis of carboxylic acids **13a-d**, **18a-d** and **23**

Aqueous solution of NaOH (1 M, 6 equiv.) was added to a solution of methyl ester **12a-d**, **17a-d** or **22** in MeOH (0.05 M). The mixture was refluxed for 30 min and MeOH was removed under reduced pressure. Aqueous solution of HCl (1 M) was added until pH reached 1. The aqueous layer was extracted with AcOEt (3 × 50 mL). The combined organic layers were dried over $MgSO_4$ and evaporated to afford carboxylic acid **13a-d**, **17a-d** or **22** which was used in the next step without further purification.

**Compound 13a.** White solid (862 mg, 93% yield, white solid). $^1$H NMR (400 MHz, MeOD, 298 K): $\delta$ ppm = 7.76 (s, 1H), 5.23 (s, 2H), 2.71 (t, 2H, $^3J$ = 7.7 Hz), 1.70−1.63 (m, 2H), 1.44−1.35 (m, 2H), 0.95 (t, 3H, $^3J$ = 7.4 Hz). $^{13}$C NMR (100 MHz, MeOD, 298 K): $\delta$ ppm = 169.9, 149.3, 124.7, 51.5, 32.7, 25.9, 23.2, 14.1. MS (ESI): $[M-H]^-$ calcd for $C_8H_{12}N_3O_2^-$: 182.1; found: 182.1.

**Compound 13b.** White solid (1.50 g, 87% yield). $^1$H NMR (400 MHz, MeOD, 298 K): $\delta$ ppm = 7.75 (s, 1H), 5.22 (s, 2H), 2.71 (t, 2H, $^3J$ = 7.6 Hz), 1.74−1.62 (m, 2H), 1.42−1.28 (m, 6H), 0.90 (t, 3H, $^3J$ = 7.0 Hz). $^{13}$C NMR (100 MHz, MeOD, 298 K): $\delta$ ppm = 169.9, 149.3, 124.7, 51.6, 32.7, 30.5, 29.9, 26.2, 23.6, 14.4. MS (ESI): $[M-H]^-$ calcd for $C_{10}H_{16}N_3O_2^-$: 210.1; found: 210.1.

**Compound 13c.** White solid (1.95 g, 89% yield). $^1$H NMR (400 MHz, MeOD, 298 K): $\delta$ ppm = 7.75 (s, 1H), 5.22 (s, 2H), 2.71 (t, 2H, $^3J$ = 7.6 Hz), 1.74−1.62 (m, 2H), 1.43−1.23 (m, 10H), 0.95 (t, 3H, $^3J$ = 6.9 Hz). $^{13}$C NMR (100 MHz, MeOD, 298 K): $\delta$ ppm = 169.9, 149.3, 124.7, 51.6, 33.0, 30.5, 30.4, 30.3, 30.2, 26.2, 23.7, 14.4. MS (ESI): $[M-H]^-$ calcd for $C_{12}H_{20}N_3O_2^-$: 238.2; found: 238.1.

**Compound 13d.** White solid (922 mg, 99% yield). $^1$H NMR (400 MHz, MeOD, 298 K): $\delta$ ppm = 8.34 (s, 1H), 7.84−7.81 (m, 2H), 7.46−7.41 (m, 2H), 7.37−7.33 (m, 1H), 5.33 (s, 2H). $^{13}$C NMR (100 MHz, MeOD, 298 K): $\delta$ ppm = 169.8, 148.9, 131.6, 130.0 (2C), 129.4, 126.7 (2C), 123.7, 51.7. Spectral data are in agreement with those previously reported in the literature.[22]

**Compound 18a.** White solid (81 mg, 84% yield). $^1$H NMR (400 MHz, MeOD, 298 K): $\delta$ ppm = 7.54 (s, 1H), 5.21 (s, 2H), 2.67 (t, 2H, $^3J$ = 7.7 Hz), 1.73−1.62 (m, 2H), 1.49−1.37 (m, 2H), 0.97 (t, 3H, $^3J$ = 7.4 Hz). $^{13}$C NMR (100 MHz, MeOD, 298 K): $\delta$ ppm = 169.8, 140.7, 132.6, 49.5 (partially masked by MeOD signal), 30.9, 23.4, 23.3, 14.0. MS (ESI): $[M-H]^-$ calcd for $C_8H_{12}N_3O_2^-$: 182.1; found: 182.1.

**Compound 18b.** White solid (64 mg, 79% yield). $^1$H NMR (400 MHz, MeOD, 298 K): $\delta$ ppm = 7.54 (s, 1H), 5.21 (s, 2H), 2.66 (t, 2H, $^3J$ = 7.7 Hz), 1.73−1.64 (m, 2H), 1.47−1.31 (m, 6H), 0.92 (t, 3H, $^3J$ = 7.0 Hz). $^{13}$C NMR (100 MHz, MeOD, 298 K): $\delta$ ppm = 169.8, 140.7, 132.6, 49.5 (partially masked by MeOD signal), 32.6, 29.9, 28.8, 23.7, 23.6, 14.4. $[M-H]^-$ calcd for $C_{10}H_{16}N_3O_2^-$: 210.1; found: 210.0.

**Compound 18c.** White solid (142 mg, 100% yield). $^1$H NMR (400 MHz, MeOD, 298 K): $\delta$ ppm = 7.54 (s, 1H), 5.21 (s, 2H), 2.66 (t, 2H, $^3J$ = 7.8 Hz), 1.72−1.65 (m, 2H), 1.44−1.26 (m, 10H), 0.90 (t, 3H, $^3J$ = 6.8 Hz). $^{13}$C NMR (100 MHz, MeOD, 298 K): $\delta$ ppm = 169.8, 140.7, 132.6, 49.5 (partially masked by MeOD signal), 33.0, 30.3 (2C), 30.2, 28.8, 23.7 (2C), 14.4. MS (ESI): $[M-H]^-$ calcd for $C_{12}H_{20}N_3O_2^-$: 238.2; found: 238.1.

**Compound 18d.** White solid (129 mg, 100% yield). $^1$H NMR (400 MHz, MeOD, 298 K): $\delta$ ppm = 7.82 (s, 1H), 7.53−7.47 (m, 5H), 5.23 (s, 2H). $^{13}$C NMR (100 MHz, MeOD, 298 K): $\delta$ ppm = 169.9, 140.7, 133.5, 130.9, 130.3 (2C) 129.8 (2C), 127.7, 50.3. MS (ESI): $[M-H]^-$ calcd for $C_{10}H_8N_3O_2^-$: 202.1; found: 202.1.

**Compound 23.** White solid (500 mg, 87% yield). $^1$H NMR (400 MHz, DMSO-$d_6$, 298 K): $\delta$ ppm = 8.11 (d, 1H, $^3J$ = 1 Hz), 7.74 (d, 1H, $^3J$ = 1 Hz), 5.29 (s, 2H). $^{13}$C NMR (100 MHz, DMSO-$d_6$, 298 K): $\delta$ ppm = 168.7, 133.2, 126.3, 50.3. MS (ESI): $[M-H]^-$ calcd for $C_4H_4N_3O_2^-$: 126.0; found: 126.0.

### 4.8. Synthesis of HMBP **8a-d**, **9a-d** and **19**

$(COCl)_2$ (1.8 eq.) was added to a solution of carboxylic acid **13a-d**, **17a-d** or **22** in dry DCM (0.44 M) at 0 °C under argon atmosphere. The mixture was stirred for 15 min and the solvent was evaporated under reduced pressure at 0 °C. The residue was dried under high vacuum to afford the corresponding acyl chloride which was immediately engaged in the next step without further purification. $P(OSiMe_3)_3$ (3.0 eq.) was slowly added to a cooled solution of acyl chloride in dry THF (0.24 M). The mixture was stirred for 20 min at 0 °C and for 30 min at room temperature. The solvent was removed under reduced pressure to afford the crude phosphonosilaester which was solubilized in dry MeOH (0.14 M). The mixture was stirred for 16 h at room temperature and evaporated. Crude compound was dissolved in a minimum amount of MeOH and this solution was added dropwise to a large volume of dry acetone under stirring. The white precipitate was collected and washed with acetone to afford the pure HMBP. Freshly prepared 0.2 M aqueous solution of NaOH (2.0 eq.) was added to a solution of the corresponding HMBP in water (0.07 M). The pH of the resulting solution is ≈ 4.5. The mixture was freeze-dried to yield HMBP **8a-d**, **9a-d** or **18** as a disodium salt.

**Compound 8a.** White solid (371 mg, 46% yield, purity ≥ 98%). $^1$H NMR (400 MHz, $D_2O$, 298 K): $\delta$ ppm = 7.81 (s, 1H), 4.83 (t, 2H, $^3J$ = 9.7 Hz, partially masked by $H_2O$ signal), 2.65 (t, 2H, $^3J$ = 7.5 Hz), 1.62−1.54 (m, 2H), 1.32−1.23 (m, 2H), 0.85 (t, 3H $^3J$ = 7.4 Hz). $^{31}$P NMR (162 MHz, $D_2O$, 298 K): $\delta$ ppm = 14.2 (br s). $^{13}$C NMR (100 MHz, $D_2O$, 298 K): $\delta$ ppm = 147.8, 125.1, 73.2 (t, $^1J$ = 133 Hz), 53.2, 30.7, 24.1, 21.3, 13.0. HRMS (ESI): [M-2Na + H]$^-$ calculated for $C_8H_{16}N_3O_7P_2^-$: 328.0469; found 328.0465.

**Compound 8b.** White solid (89 mg, 47%, yield, purity ≥ 98%). $^1$H NMR (400 MHz, $D_2O$, 298 K): $\delta$ ppm = 7.87 (s, 1H), 4.90−4.85 (m, 2H), 2.69 (t, 2H, $^3J$ = 7.5 Hz), 1.68−1.60 (m, 2H), 1.34−1.23 (m, 6H),

0.84 (t, 3H, $^3J$ = 7.0 Hz). $^{31}$P NMR (162 MHz, $D_2O$, 298 K): $\delta$ ppm = 14.1 (br s). $^{13}$C NMR (100 MHz, $D_2O$, 298 K): $\delta$ ppm = 148.0, 125.0, 73.3 (t, $^1J$ = 134 Hz), 53.2, 30.7, 28.5, 27.8, 24.4, 21.9, 13.3. HRMS (ESI): [M-2Na + H]$^-$ calculated for $C_{10}H_{20}N_3O_7P_2^-$: 356.0782; found 356.0784.

**Compound 8c.** White solid (36 mg, 40% yield, purity ≥ 98%). $^1$H NMR (400 MHz, $D_2O$, 298 K): $\delta$ ppm = 7.83 (s, 1H), 4.88–4.84 (m, 2H, partially masked by $H_2O$ signal), 2.67 (t, 2H, $^3J$ = 7.2 Hz), 1.70–1.56 (m, 2H), 1.37–1.17 (m, 10H), 0.83 (t, 3H, $^3J$ = 6.4 Hz). $^{31}$P NMR (162 MHz, $D_2O$, 298 K): $\delta$ ppm = 14.2 (t, $^3J$ = 9.7 Hz). $^{13}$C NMR (100 MHz, $D_2O$, 298 K): $\delta$ ppm = 148.0, 125.0, 73.3 (t, $^1J$ = 133 Hz), 53.2, 31.1, 28.5, 28.4, 28.3, 28.1, 24.4, 22.0, 13.4. HRMS (ESI): [M-2Na + H]$^-$ calculated for $C_{12}H_{24}N_3O_7P_2^-$: 384.1095; found 384.1095.

**Compound 8d.** White solid (380 mg, 44% yield, purity ≥ 98%). $^1$H NMR (400 MHz, $D_2O$, 298 K): $\delta$ ppm = 8.36 (s, 1H), 7.82–7.79 (m, 2H), 7.51–7.47 (m, 2H), 7.43–7.39 (m, 1H), 4.96–4.91 (m, 2H). $^{31}$P NMR (162 MHz, $D_2O$, 298 K): $\delta$ ppm = 14.1 (br s). $^{13}$C NMR (100 MHz, $D_2O$, 298 K): $\delta$ ppm = 146.6, 129.8, 129.1 (2C), 128.5, 125.6 (2C), 124.1, 73.3 (t, $^1J$ = 133 Hz), 53.5. Spectral data are in agreement with those previously reported in the literature.[23]

**Compound 9a.** White solid (80 mg, 39% yield, purity ≥ 98%). $^1$H NMR (400 MHz, $D_2O$, 298 K): $\delta$ ppm = 7.54 (s, 1H), 4.82–4.77 (m, 2H, masked by HDO signal), 2.82 (t, 2H, $^3J$ = 7.7 Hz), 1.66–1.58 (m, 2H), 1.39–1.30 (m, 2H), 0.89 (t, 3H, $^3J$ = 7.4 Hz). $^{31}$P NMR (162 MHz, $D_2O$, 298 K): $\delta$ ppm = 14.1 (br s). $^{13}$C NMR (100 MHz, $D_2O$, 298 K): $\delta$ ppm = 141.3, 131.4, 73.6 (t, $^1J$ = 133 Hz), 49.9, 29.4, 22.4, 21.6, 13.0. HRMS (ESI): [M-2Na + H]$^-$ calculated for $C_8H_{16}N_3O_7P_2^-$: 328.0469; found 328.0469.

**Compound 9b.** White solid (61 mg, 55% yield, purity ≥ 98%). $^1$H NMR (400 MHz, $D_2O$, 298 K): $\delta$ ppm = 7.65 (s, 1H), 4.88–4.83 (m, 2H), 2.87 (t, 2H, $^3J$ = 7.6 Hz), 1.71–1.64 (m, 2H), 1.38–1.28 (m, 6H), 0.86 (t, 3H, $^3J$ = 6.5 Hz). $^{31}$P NMR (162 MHz, $D_2O$, 298 K): $\delta$ ppm = 14.1 (br s). $^{13}$C NMR (100 MHz, $D_2O$, 298 K): $\delta$ ppm = 141.9, 130.7, 73.5 (t, $^1J$ = 134 Hz), 50.4, 30.7, 27.9, 27.1, 22.7, 21.8, 13.3. HRMS (ESI): [M-2Na + H]$^-$ calculated for $C_{10}H_{20}N_3O_7P_2^-$: 356.0782; found 356.0781.

**Compound 9c.** White solid (41 mg, 24% yield, purity ≥ 98%). $^1$H NMR (400 MHz, $D_2O$, 298 K): $\delta$ ppm = 7.53 (s, 1H), 4.89–4.72 (m, 2H, masked by HDO signal), 2.83 (t, 2H, $^3J$ = 6.6 Hz), 1.69–1.58 (m, 2H), 1.40–1.15 (m, 10H), 0.88–0.77 (m, 3H). $^{31}$P NMR (162 MHz, $D_2O$, 298 K): $\delta$ ppm = 14.0 (t, $^3J$ = 9.1 Hz). $^{13}$C NMR (100 MHz, $D_2O$, 298 K): $\delta$ ppm = 141.2, 131.5, 73.6 (t, $^1J$ = 132 Hz), 50.1, 28.4, 28.3 (2C), 28.2, 27.2, 22.7, 22.0, 13.4. HRMS (ESI): [M − Na]$^-$ calculated for $C_{12}H_{23}N_3O_7P_2Na^-$: 406.0914; found 406.0928.

**Compound 9d.** White solid (85 mg, 43% yield, purity ≥ 98%). $^1$H NMR (400 MHz, $D_2O$, 298 K): $\delta$ ppm = 7.78 (s, 1H), 7.61–7.50 (m, 5H), 4.95 (t, 2H, $^3J$ = 9.4 Hz). $^{31}$P NMR (162 MHz, $D_2O$, 298 K): $\delta$ ppm = 14.0 (br s). $^{13}$C NMR (100 MHz, $D_2O$, 298 K): $\delta$ ppm = 140.3, 132.7, 129.6, 129.4 (2C),128.9 (2C), 126.6, 73.8 (t, $^1J$ = 135 Hz), 50.7. HRMS (ESI): [M-2Na + H]$^-$ calculated for $C_{10}H_{12}N_3O_7P_2^-$: 348.0156; found 348.0155.

**Compound 19.** White solid (153 mg, 48% yield, purity ≥ 98%). A catalytic amount of DMF (1 drop) was required for the efficient conversion of **23** into the corresponding acyl chloride. $^1$H NMR (400 MHz, $D_2O$, 298 K): $\delta$ ppm = 8.05 (s, 1H), 7.71 (s, 1H), 4.91 (t, 2H, $^3J$ = 9.6 Hz, $H_2$). $^{31}$P NMR (162 MHz, $D_2O$, 298 K): $\delta$ ppm = 14.1 (br s). $^{13}$C NMR (100 MHz, $D_2O$, 298 K): $\delta$ ppm = 133.1, 127.5, 73.2 (t, $^1J$ = 133 Hz), 53.2. HRMS (ESI): [M-2Na + H]$^-$ calculated for $C_4H_8N_3O_7P_2^-$: 271.9843; found 271.9847.

### 4.9. Cell culture

MIA PaCa-2 (human pancreatic carcinoma), MDA-MB-231 (human breast adenocarcinoma) and A549 (human lung carcinoma) cell lines were obtained from the American Type Culture Collection (ATCC). These cells were grown in high glucose Dulbecco's modified Eagle's medium (DMEM − Sigma Aldrich) supplemented with 10% fetal bovine serum and 1% penicillin/streptomycin (Sigma Aldrich) in a standard humified incubator at 37 °C and 5% $CO_2$.

### 4.10. Cell viability

Cell viability was evaluated using the MTT colorimetric assay. MIA PaCa-2, A549 and MDA-MB-231 cells were seeded respectively at a density of $1 \times 10^3$, $1 \times 10^3$ and $4 \times 10^3$ cells/well in a 96-well plate in DMEM supplemented with 10% fetal bovine serum and 1% penicillin/streptomycin. 24 h later, the culture medium was removed and replaced by 100 μL of culture medium containing increasing concentrations of test compound (0.1–100 μM). After 72 h incubation, 10 μL of the MTT solution (5 mg/mL in PBS) were added to each well. After additional 3 h of incubation, the culture medium was removed, and the insoluble purple product was dissolved by addition of DMSO (50 μL). Optical density was measured at 570 nm using a Thermo Scientific Multiskan FC microplate reader. Concentration of bisphosphonate required for 50% decrease in cell viability ($IC_{50}$) were determined by using GraphPad software. These experiments were carried out at least 3 times in triplicate.

### 4.11. In-vitro inhibition of FPP/GPP biosynthesis

The inhibition of FPP/GGPP biosynthesis was studied by treating MIA PaCa-2 cells with **8b** (2 μM) in the presence or absence of FOH (50 μM) or GGOH (50 μM). MIA PaCa-2 cells were seeded at a density of $1 \times 10^3$ cells/well in a 96-well plate in DMEM supplemented with 10% fetal bovine serum and 1% penicillin/streptomycin. After 24 h incubation at 37 °C and 5% $CO_2$, the culture medium was replaced with fresh medium containing tested compounds (100 μL). After 72 h of treatment, 10 μL of the MTT solution (5 mg/mL in PBS) were added to each well. Cells were further incubated for 3 h at 37 °C. Then the culture medium was removed, and the insoluble product was dissolved by addition of DMSO (50 μL) before determination of the absorbance at 570 nm. Cell viability was determined by using GraphPad software. These experiments were performed 3 times in triplicate.

### 4.12. Computational investigations

All docking computations were performed with the Autodock software [40]. Compounds **8a-d** and **9a-d** were built with the help of maestro Schrödinger program [41]. The coordinates of human GGPPS were found in the pdb with the accession code 6C57 [14]. After a molecular dynamics stage (see ESI) a grid box of $62 \times 68 \times 54$ Å$^3$ was designed around the magnesium ions to delineate the binding pocket for the molecular docking computations. 200 cycles of calculations were performed in order to get a final docking pose as accurate as possible. The resulting docking structures were then clustered and the conformation selected was the one which presented the lowest docking free energy of binding in the most populated cluster [42]. [43] Visualization, structural alignment and analysis of protein–ligand interactions were made with the help of the visual molecular dynamic [44] software and hydrophobicity surface coloration with Eisenberg scale computations [45].

The authors declare that they have no known competing financial interests or personal relationships that could have appeared to influence the work reported in this paper.

## Declaration of competing interest

The authors declare that they have no known competing financial interests or personal relationships that could have

appeared to influence the work reported in this paper.

## Acknowledgements

We gratefully acknowledge the Centre National pour la Recherche Scientifique (CNRS), Université Sorbonne Paris Nord (BQR 2019 grant), La Ligue Nationale Contre le Cancer (Comité Val-de-Marne) and GDR Phosphore (2008, CNRS) for their financial support. M.A.R. thanks the Algeria Ministry of Higher Education and Scientific Research for Profas B+ fellowship. A. D thanks the Ministère de l'Enseignement Supérieur et de la Recherche (MESR) for PhD fellowship.

## Appendix A. Supplementary data

Supplementary data to this article can be found online at https://doi.org/10.1016/j.ejmech.2021.113241.

| a)fx278 | b) fx279 |
|---|---|

Figure S1: a) HSQC NMR spectrum of a 1,4-disubstituted triazole 12b. b) HSQC NMR spectrum of a1,4- disubstituted triazole 17b.

## References

[1] R.G.G. Russel, Bisphosphonates: the first 40 years, Bone 49 (2011) 2–19, https://doi.org/10.1016/j.bone.2011.04.022.

[2] M.C. Winter, I. Holen, R.E. Coleman, Exploring the anti-tumour activity of bisphosphonates in early breast cancer, Canc. Treat Rev. 34 (2008) 453–475, https://doi.org/10.1016/j.ctrv.2008.02.004.

[3] S. Matsumoto, S. Kimura, H. Segawa, J. Kuroda, T. Yuasa, K. Sato, M. Nogawa, F. Tanaka, T. Maekawa, H. Wada, Efficacy of the third-generation bisphosphonate, zoledronic acid alone and combined with anti-cancer agents against small cell lung cancer cell lines, Lung Canc. 47 (2005) 31–39, https://doi.org/10.1016/j.lungcan.2004.06.003.

[4] M.V. Lee, E.M. Fong, F.R. Singer, R.S. Guenette, Bisphosphonate treatment inhibits the growth of prostate cancer cells, Canc. Res. 61 (2001) 2602–2608.

[5] a) C.M. Shipman, M.J. Rogers, J.F. Apperley, R.G.G. Russel, P.I. Croucher, Bisphosphonates induce apoptosis in human myeloma cell lines: a novel anti-tumour activity, Br. J. Haematol. 98 (1997) 665–672, https://doi.org/10.1046/j.1365-2141.1997.2713086.x;
b) A.U. Ural, M.I. Yilmaz, F. Avcu, A. Pekel, M. Zerman, O. Nevruz, A. Sengul, A. Yalcin, The bisphosphonate zoledronic acid induces cytotoxicity in human myeloma cell lines with enhancing effects of dexamethasone and thalidomide, Int. J. Hematol. 78 (2003) 443–449, https://doi.org/10.1007/BF02983818.

[6] J. Zekri, M. Mansour, S.M. karim, The anti-tumour effect of zoledronic acid, J. Bone Oncol. 3 (2014) 25–35, https://doi.org/10.1016/j.jbo.2013.12.001.

[7] a) R.E. Coleman, H. Marshall, D. Cameron, D. Dodwell, R. Burkinshaw, M. Keane, M. Gil, S.J. Houston, R.J. Grieve, P.J. Barrett-Lee, D. Ritchie, J. Pugh, C. Gaunt, U. Rea, J. Peterson, C. Davies, Victoria Hiley, W. Gregory, R. Bell, Breast-cancer adjuvant therapy with zoledronic acid, N. Engl. J. Med. 365 (2011) 1396–1405, https://doi.org/10.1056/NEJMoa1105195;
b) R. Coleman, D. Cameron, D. Dodwell, R. Bell, C. Wilson, E. Rathbone, M. Keane, M. Gil, R. Burkinshaw, R. Grieve, P. Barrett-Lee, D. Ritchie, V. Liversedge, S. Hinsley, H. Marshall, Adjuvant zoledronic acid in patients with early breast cancer: final efficacy analysis of the AZURE (BIG 01/04) randomised open-label phase 3 trial, Lancet Oncol. 15 (2014) 997–1006, https://doi.org/10.1016/S1470-2045(14)70302-X;
c) R. Coleman, R. de Boer, H. Eidtmann, A. Llombart, N. Davidson, P. Neven, G. von Minckwitz, H.P. Sleeboom, J. Forbes, C. Barrios, A. Frassoldati, I. Campbell, O. Paija, N. Martin, A. Modi, N. Bundred, Zoledronic acid (zoledronate) for postmenopausal women with early breast cancer receiving adjuvant letronazole (ZO-FAST study): final 60 months results, Ann. Oncol. 24 (2013) 398–405, https://doi.org/10.1093/annonc/mds277;
d) M. Gnant, B. Mlineritsch, W. Schippinger, G. Luschin-Ebengreuth, S. Pöstlberger, C. Menzel, R. Jakesz, M. Seifert, M. Hubalek, V. Bjelic-Radisic, H. Samonigg, C. Tausch, H. Eidtmann, G. Steger, W. Kwasny, P. Dubsky, M. Fridrik, F. Fitzal, M. Stierer, E. Rücklinger, R. Greil, Endocrine therapy plus zoledronic acid in premenopausal breast cancer, N. Engl. J. Med. 360 (2009) 679–691, https://doi.org/10.1056/NEJMoa0806285;
e) M. Gnant, B. Mlineritsch, H. Stoeger, G. Luschin-Ebengreuth, D. Heck, C. Menzel, R. Jakesz, M. Seifert, M. Hubalek, G. Pristauz, T. Bauernhofer, H. Eidtmann, W. Eiermann, G. Steger, W. Kwasny, P. Dubsky, G. Hochreiner, E.-P. Forsthuber, C. Fesl, R. Greil, Adjuvant endocrine therapy plus zoledronic acid in premenopausal women with early-stage breast cancer: 62-month follow-up from the ABCSG-12 randomised trial, Lancet Oncol. 12 (2011) 631–641, https://doi.org/10.1016/S1470-2045(11)70122-X.

[8] G. J Morgan, F.E. Davies, W.M. Gregory, K. Cocks, S.E. Bell, A.J. Szubert, N. Navarro-Coy, M.T. Drayson, R.G. Owen, S. Feyler, A.J. Ashcroft, F. Ross, J. Byrne, H. Roddie, C. Rudin, G. Cook, G.H. Jackson, J.A. Child, First-line treatment with zoledronic acid as compared with clodronic acid in multiple myeloma (MRC Myeloma IX): a randomised controlled trial, Lancet 376 (2010) 1989–1999, https://doi.org/10.1016/S0140-6736(10)62051-X.

[9] a) J.E. Dunford, K. Thompson, F.P. Coxon, S.P. Luckman, F.M. Hahn, C.D. Poulter, F.H. Ebetino, M.J. Rogers, Structure-activity relationships for inhibition of farnesyl diphosphate synthase in vitro and inhibition of bone resorption in vivo by nitrogen-containing bisphosphonates, J. Pharmacol. Exp. Therapeut. 296 (2001) 235–242;
b) J.-M. Rondeau, F. Bitsch, E. Bourgier, M. Geiser, R. Hemmig, M. Kroemer, S. Lehmann, P. Ramage, S. Rieffel, A. Strauss, J.R. Green, W. Jahnke, Structural basis for the exceptional in vivo efficacy of bisphosphonate drugs, ChemMedChem 1 (2006) 267–273, https://doi.org/10.1002/cmdc.200500059;
c) K.L. Kavanagh, K. Guo, J.E. Dunford, X. Wu, S. Knapp, F.H. Ebetino, M.J. Rogers, R.G.G. Russell, U. Oppermann, The molecular mechanism of nitrogen-containing bisphosphonates as antiosteoporosis drugs, Proc. Natl. Acad. Sci. U.S.A. 103 (2006) 7829–7834, https://doi.org/10.1073/pnas.0601643103.

[10] K.L. Kavanagh, J.E. Dunford, G. Bunkoczi, R.G.G. Russell, U. Oppermann, The crystal structure of human geranylgeranyl pyrophosphate synthase reveals a novel hexameric arrangement and inhibitory product binding, J. Biol. Chem. 281 (2006) 22004–22012, https://doi.org/10.1074/jbc.M602603200.

[11] J.E. Dunford, A.A. Kwaasi, M.J. Rogers, B.L. Barnett, F.H. Ebetino, R.G.G. Russell, U. Oppermann, K.L. Kavanagh, Structure–activity relationships among the nitrogen containing bisphosphonates in clinical use and other analogues: time-dependent inhibition of human farnesyl pyrophosphate synthase, J. Med. Chem. 51 (2008) 2187–2195, https://doi.org/10.1021/jm7015733.

[12] M.B. Martin, W. Arnold, H.T. Heath III, J.A. Urbina, E. Oldfield, Nitrogen-containing bisphosphonates as carbocation transition state analogs for isoprenoid biosynthesis, Biochem. Biophys. Res. Commun. 263 (1999) 754–758, https://doi.org/10.1006/bbrc.1999.1404.

[13] a) S.L. Haney, V.S. Wills, D.F. Wiemer, S.A. Holstein, Recent advances in the development of mammalian geranylgeranyl diphosphate synthase inhibitors, Molecules 22 (2017) 886, https://doi.org/10.3390/molecules22060886;
b) D.D. Waller, J. Park, Y.S. Tsantrizos, Inhibition of farnesyl pyrophosphate (FPP) and/or geranylgeranyl pyrophosphate (GGPP) biosynthesis and its implication in the treatment of cancers, Crit. Rev. Biochem. Mol. Biol. 54 (2019) 41–60, https://doi.org/10.1080/10409238.2019.1568964.

[14] C.M. Lacbay, D.D. Waller, J. Park, M. Gómez Palou, F. Vincent, X. Fang Huang, V. Ta, A.M. Berghuis, M. Sebag, Y.S. Tsantrizos, Unraveling the prenylation–cancer paradox in multiple myeloma with novel geranylgeranyl pyrophosphate synthase (GGPPS) inhibitors, J. Med. Chem. 61 (2018) 6904–6917, https://doi.org/10.1021/acs.jmedchem.8b00886.

[15] a) L.W. Shull, A.J. Wiemer, R.J. Hohl, D.F. Wiemer, Synthesis and biological activity of isoprenoid bisphosphonates, Bioorg. Med. Chem. 14 (2006) 4130–4136, https://doi.org/10.1016/j.bmc.2006.02.010;
b) A.J. Wiemer, H. Tong, K.M. Swanson, R.J. Hohl, Digeranyl bisphosphonate inhibits geranylgeranyl pyrophosphate synthase, Biochem. Biophys. Res. Commun. 353 (2007) 921–925, https://doi.org/10.1016/j.bbrc.2006.12.094.

[16] Y. Zhang, R. Cao, F. Yin, M.P. Hudock, R.-T. Guo, K. Krysiak, S. Mukherjee, Y.-G. Gao, H. Robinson, Y. Song, J.H. No, K. Bergan, A. Leon, L. Cass, A. Goddard, T.-K. Chang, F.-Y. Lin, E. Van Beek, S. Papapoulos, A.H.-J. Wang, T. Kubo, M. Ochi, D. Mukkamala, E. Oldfield, Lipophilic bisphosphonates as dual farnesyl/geranylgeranyl diphosphate synthase inhibitors: an X-ray and NMR investigation, J. Am. Chem. Soc. 131 (2009) 5153–5162, https://doi.org/10.1021/ja808285e.

[17] C. Allen, S. Kortagere, H. Tong, R.A. Matthiesen, J.I. Metzger, D.F. Wiemer, S.A. Holstein, Olefin isomers of a triazole bisphosphonate synergistically inhibit geranylgeranyl diphosphate synthase, Mol. Pharmacol. 91 (2017) 229–236, https://doi.org/10.1124/mol.116.107326.

[18] V.S. Wills, C. Allen, S.A. Holstein, D.F. Wiemer, Potent triazole bisphosphonate inhibitor of geranylgeranyl diphosphate synthase, ACS Med. Chem. Lett. 6 (2015) 1195–1198, https://doi.org/10.1021/acsmedchemlett.5b00334.

[19] S.L. Haney, M.L. Varney, Y.S. Chhonker, S. Shin, K. Mehla, A.J. Crawford, H. Jensen Smith, L.M. Smith, D.J. Murry, M.A. Hollingsworth, S.A. Holstein, Inhibition of geranylgeranyl diphosphate synthase is a novel therapeutic strategy for pancreatic ductal adenocarcinoma, Oncogene 38 (2019) 5308–5320, https://doi.org/10.1038/s41388-019-0794-6.

[20] X. Zhou, S.D. Ferree, V.S. Wills, E.J. Born, H. Tong, D.F. Wiemer, S.A. Holstein, Geranyl and neryl triazole bisphosphonates as inhibitors of geranylgeranyl diphosphate synthase, Bioorg. Med. Chem. 22 (2014) 2791–2798, https://doi.org/10.1016/j.bmc.2014.03.014.

[21] V.S. Wills, J.I. Metzger, C. Allen, M.L. Varney, D.F. Wiemer, S.A. Holstein, Bishomoprenoid triazole bisphosphonates as inhibitors of geranylgeranyl diphosphate synthase, Bioorg. Med. Chem. 25 (2017) 2437–2444, https://doi.org/10.1016/j.bmc.2017.02.066.

[22] a) E. Guenin, D. Ledoux, O. Oudar, M. Lecouvey, M. Kraemer, Structure-activity relationships of a new class of aromatic bisphosphonates that inhibit tumor cell proliferation in vitro, Anticancer Res. 25 (2005) 1139–1146;
b) S. Muller, E. Migianu, M. Lecouvey, M. Kraemer, O. Oudar, Alendronate inhibits proliferation and invasion of human epidermoid carcinoma cells in vitro, Anticancer Res. 25 (2005) 2655–2660;
c) M. Abdelkarim, E. Guenin, O. Sainte-Catherine, N. Vintonenko, N. Peyri, G.Y. Perret, M. Crepin, A.-M. Khatib, M. Lecouvey, M. Di Benedetto, New symmetrically esterified m-bromobenzyl non-aminobisphosphonates inhibited breast cancer growth and metastases, PloS One 4 (2009) e4685, https://doi.org/10.1371/journal.pone.0004685;
d) M. Monteil, E. Migianu-Griffoni, O. Sainte-Catherine, M. Di Benedetto, M. Lecouvey, Bisphosphonate prodrugs: synthesis and biological evaluation in HuH 7 hepatocarcinoma cells, Eur. J. Med. Chem. 77 (2014) 56–64, https://doi.org/10.1016/j.ejmech.2014.02.054;
e) E. Migianu-Griffoni, I. Chebbi, S. Kachbi, M. Monteil, O. Sainte-Catherine, F. Chaubet, O. Oudar, M. Lecouvey, Synthesis and biological evaluation of new bisphosphonate–dextran conjugates targeting breast primary tumor, Bioconjugate Chem. 25 (2014) 224–230, https://doi.org/10.1021/bc400317h.

[23] M. Lv, M. Wang, K. Lu, L. Peng, Y. Zhao, Synthesis and characterization of novel 1,2,3-triazoles containing a 1-hydroxyalkane-1,1-bisphosphonate substituent. *Phosphorus, Sulfur, Silicon Relat*, Elements 193 (2018) 206–210, https://doi.org/10.1080/10426507.2017.1417299.

[24] R.A. Matthiesen, V.S. Wills, J.I. Metzger, S.A. Holstein, D.F. Wiemer, Stereoselective synthesis of homoneryl and homogeranyl triazole bisphosphonate, J. Org. Chem. 81 (2016) 9438–9442, https://doi.org/10.1021/acs.joc.6b01693.

[25] a) D. Dheer, V. Singh, R. Shankar, Medicinal attributes of 1,2,3-triazoles: current developments, Bioorg. Chem. 71 (2017) 30–54, https://doi.org/10.1016/j.bioorg.2017.01.010;
b) X. Jiang, X. Hao, L. Jing, G. Wu, D. Kang, X. Liu, P. Zhan, Recent applications of click chemistry in drug discovery, Expet Opin. Drug Discov. 14 (2019) 779–789, https://doi.org/10.1080/17460441.2019.1614910;
c) K. Bozorov, J. Zhao, H.A. Aisa, 1,2,3-Triazole containing hybrids as leads in medicinal chemistry: a recent overview, Bioorg. Med. Chem. 27 (2019) 3511–3531, https://doi.org/10.1016/j.bmc.2019.07.005.

[26] E. Bonandi, M.S. Christodoulou, G. Fumagalli, D. Perdicchia, G. Rastelli, D. Passarella, The 1,2,3-triazole ring as a bioisostere in medicinal chemistry, Drug Discov. Today 22 (2017) 1572–1581, https://doi.org/10.1016/j.drudis.2017.05.014.

[27] a) V.V. Rostovtsev, L.G. Green, V.V. Fokin, K.B. Sharpless, A stepwise Huisgen cycloaddition process: copper(I)-catalyzed regioselective "ligation" of azides and terminal alkynes, Angew. Chem. Int. Ed *41* (2002) 2596–2599. 10.1002/1521-3773(20020715)41:14<2596::AID-ANIE2596>3.0.CO;2-4;
b) C.W. Tornøe, C. Christensen, M. Meldal, Peptidotriazoles on solid phase: [1,2,3]-triazoles by regiospecific copper(I)-catalyzed 1,3-dipolar cycloadditions of terminal alkynes to azides, J. Org. Chem. 67 (2002) 3057–3064, https://doi.org/10.1021/jo011148j.

[28] a) G.R. Kieczykowski, R.B. Jobson, D.G. Melillo, D.F. Reinhold, V.J. Grenda, I. Shinkai, Preparation of (4-amino-l-hydroxybutylidene)bisphosphonic acid sodium salt, MK-217 (alendronate sodium). An improved procedure for the preparation of 1-hydroxy-1,1-bisphosphonic acids, J. Org. Chem. 60 (1995) 8310–8312, https://doi.org/10.1021/jo00130a036;
b) J. Dussart, J. Deschamp, E. Migianu-Griffoni, M. Lecouvey, From industrial method to the use of silylated P(III) reagents for the synthesis of relevant phosphonylated molecules, Org. Process Res. Dev. 24 (2020) 637–651, https://doi.org/10.1021/acs.oprd.9b00490.

[29] M. Lecouvey, I. Mallard, T. Bailly, R. Burgada, Y. Leroux, A mild and efficient one-pot synthesis of 1-hydroxymethylene-1,1-bisphosphonic acids. Preparation of new tripod ligands, Tetrahedron Lett. 42 (2001) 8475–8478, https://doi.org/10.1016/S0040-4039(01)01844-5.

[30] a) L. Zhang, X. Chen, P. Xue, H.H.Y. Sun, I.D. Williams, K.B. Sharpless, V.V. Fokin, G. Jia, Ruthenium-catalyzed cycloaddition of alkynes and organic azides, J. Am. Chem. Soc. 127 (2005) 15998–15999, https://doi.org/10.1021/ja054114;
b) B.C. Boren, S. Narayan, L.K. Rasmussen, L. Zhang, H. Zhao, Z. Lin, G. Jia, V.V. Fokin, Ruthenium-catalyzed azide-alkyne cycloaddition: scope and mechanism, J. Am. Chem. Soc. 130 (2008) 8923–8930, https://doi.org/10.1021/ja0749993.

[31] X. Creary, A. Anderson, C. Brophy, F. Crowell, Z. Funk, Method for assigning structure of 1,2,3-triazoles, J. Org. Chem. 77 (2012) 8756–8761, https://doi.org/10.1021/jo301265t.

[32] J.M. Sanders, S. Ghosh, J.M.W. Chan, G. Meints, H. Wang, A.M. Raker, Y. Song, A. Colantino, A. Burzinska, P. Kafarski, G.T. Morita, E. Oldfield, Quantitative structure-activity relationships for γδ T cell activation by bisphosphonates, J. Med. Chem. 47 (2004) 375–384, https://doi.org/10.1021/jm0303709.

[33] S. Kun, G.Z. Nagy, M. Tóth, L. Czecze, A. Nguyen Van Nhien, T. Docsa, P. Gergely, M.-D. Charavgi, P.V. Skourti, E.D. Chrysina, T. Patonay, L. Somsák, Synthesis of variously coupled conjugates of D-glucose, 1,3,4-oxadiazole, and 1,2,3-triazole for inhibition of glycogen phosphorylase, Carbohydr. Res. 346 (2011) 1427–1438, https://doi.org/10.1016/j.carres.2011.03.004.

[34] D.C. Crick, D.A. Andres, C.J. Waechter, Novel salvage pathway utilizing farnesol and geranylgeraniol for protein isoprenylation, Biochem. Biophys. Res. Commun. 237 (1997) 483–487, https://doi.org/10.1006/bbrc.1997.7145.

[35] a) S.P. Jagdev, R.E. Coleman, C.M. Shipman, A. Rostami, H. Croucher, P.I. Croucher, The bisphosphonate, zoledronic acid, induces apoptosis of breast cancer cells: evidence for synergy with paclitaxel, Brit. J. cancer 84 (2001) 1126–1134, https://doi.org/10.1054/bjoc.2001.1727;
b) C. Denoyelle, L. Hong, J.-P. Vannier, J. Soria, C. Soria, New insights into the actions of bisphosphonate zoledronic acid in breast cancer cells by dual RhoA-dependent and -independent effects, Br. J. Canc. 88 (2003) 1631–1640, https://doi.org/10.1038/sj.bjc.6600925;
c) M. Goffinet, M. Thoulouzan, A. Pradines, I. Lajoie-Mazenc, C. Weinbaum, J.C. Faye, S. Séronie-Vivien, Zoledronic acid treatment impairs protein geranylgeranylation for biological effects in prostatic cells, BMC Canc. 6 (2006) 60, https://doi.org/10.1186/1471-2407-6-60.

[36] A. Albert, P.J. Taylor, The tautomerism of 1,2,3-triazole in aqueous solution, J. Chem. Soc., Perkin trans. 2 (1989) 1903–1905, https://doi.org/10.1039/P29890001903.

[37] C.K.-M. Chen, M.P. Hudock, Y. Zhang, R.-T. Guo, R. Cao, J.H. No, P.-H. Liang, T.-P. Ko, T.-H. Chang, S.-c. Chang, Y. Song, J. Axelson, A. Kumar, A.H.-J. Wang, E. Oldfield, Inhibition of geranylgeranyl diphosphate synthase by bisphosphonates: a crystallographic and computational investigation, J. Med. Chem. 51 (2008) 5594–5607, https://doi.org/10.1021/jm800325y.

[38] H.G. Bonacorso, F.M. Libero, G.M. Dal Forno, E.P. Pittaluga, D.F. Back, M. Hörner, M.A.P. Martins, N. Zanatta, New regioselective synthesis of polyfunctionalized 3-ferrocenyl-1H-pyrroles under microwave irradiation, Tetrahedron Lett. 57 (2016) 4568–4573, https://doi.org/10.1016/j.tetlet.2016.08.088.

[39] R.L. Kimber, F. Parmeggiani, N. Joshi, A.M. Rakowski, S.J. Haigh, N.J. Turner, J.R. Lloyd, Synthesis of copper catalysts for click chemistry from distillery wastewater using magnetically recoverable bionanoparticles, Green Chem. 21 (2019) 4020–4024, https://doi.org/10.1039/C9GC00270G.

[40] G.M. Morris, R. Huey, W. Lindstrom, M.F. Sanner, R.K. Belew, D.S. Goodsell, A.J. Olson, AutoDock 4 and AutoDockTools 4: automated docking with selective receptor flexibility, J. Comput. Chem. 30 (2009) 2785–2791, https://doi.org/10.1002/jcc.21256.

[41] Schrödinger Release 2020-1: Maestro; Schrödinger, LLC: New York, NY.

[42] F. Barbault, L. Zhang, L. Zhang, B.T. Fan, Parametrization of a specific free energy function for automated docking against RNA targets using neural networks, Chemometr. Intell. Lab. Syst. 82 (2006) 269–275, https://doi.org/10.1016/j.chemolab.2005.05.014.

[43] C. Teixeira, N. Serradji, F. Maurel, F. Barbault, Docking and 3D-QSAR studies of BMS-806 analogs as HIV-1 Gp120 entry inhibitors, Eur. J. Med. Chem. 44 (2009) 3524–3532, https://doi.org/10.1016/j.ejmech.2009.03.028.

[44] W. Humphrey, A. Dalke, K. Schulten, VMD: visual molecular dynamics, J. Mol. Graph. 14 (1996) 33–38, https://doi.org/10.1016/0263-7855(96)00018-5.

[45] F. Barbault, C. Landon, M. Guenneugues, J.-P. Meyer, V. Schott, J.-L. Dimarcq, F. Vovelle, Solution structure of Alo-3: a new knottin-type antifungal peptide from the insect acrocinus longimanus, Biochemistry 42 (2003) 14434–14442, https://doi.org/10.1021/bi035400o.